A new method to characterise and model stress-relaxation ageing behaviour of an aluminium alloy under age forming conditions

Yong Li[1,2,*] and Zhusheng Shi[3,*]

[1]School of Mechanical Engineering and Automation, Beihang University, Beijing 100191, China

[2]Shenzhen Institute of Beihang University, Shenzhen 518057, China

[3]Department of Mechanical Engineering, Imperial College London, London SW7 2AZ, UK

* Corresponding authors: liyong19@buaa.edu.cn (Y. Li), zhusheng.shi@imperial.ac.uk (Z. Shi)

Abstract

A new method that utilises theories of thermally activated deformation and repeated transient stress-relaxation tests has been proposed and validated in this study for the characterisation and modelling of the stress-relaxation ageing (SRA) behaviour of aluminium alloys and its dependence on stress and temperature. Using the new method, key deformation-related variables, i.e. stress components, activation volume and energy, of the aerospace grade heat-treatable aluminium alloy AA7B04 have been obtained as a function of ageing temperature (388, 413 and 438 K), stress (both elastic and plastic) and SRA time (up to 4 h). It has been found that the apparent activation energy Q_a of the material remains constant in the elastic region but decreases with increasing strain in the plastic region, and also decreases with increasing temperature for all initial loading stresses. These characteristics contribute to a much higher degree of stress-relaxation in the plastic region and at higher temperatures than in the elastic region and/or at lower temperatures. The obtained changing activation volume V and Q_a indicate that the deformation rate is controlled by forest dislocation interactions in the elastic region (V decreases from over $200b^3$ to less than $100b^3$), and by a cross-slip mechanism at high stress levels in the plastic region (V decreases to a few tens of b^3). Based on these theories and results, a novel and simple constitutive model has been proposed, with which the stress-relaxation behaviour of AA7B04 at different ageing temperatures (388 to 448 K), pre-loaded from elastic to plastic regions for up to 16 h has been successfully predicted. The proposed model eliminates the limitations of conventional SRA models which mainly deal with elastic loading and isothermal conditions, and provides a foundation to effectively predict the springback after advanced non-isothermal SRA forming of aluminium alloy structures in the aerospace industry.

Keywords: Stress-relaxation; Stress level; Physical Activation Volume; Activation Energy; Constitutive Model; Aluminium Alloy.

1. Introduction

Stress-relaxation age forming (SRAF), also termed creep age forming (CAF), is an advanced technology for the manufacture of large panels, such as wing structural panels, in the aerospace industry; it combines thermally activated stress-relaxation (or creep) and artificial ageing to concurrently form and strengthen heat-treatable aluminium alloy components[1]. The alloys are loaded at intermediate stress levels to give either purely elastic strains, as in the case of wing skin panels, or small plastic strains (less than 5% plastic strain for stiffened panels [2]). During the loading process, the alloys are held at artificial ageing temperatures (usually less than 473 K), allowing thermally activated stress-relaxation and age strengthening processes to occur simultaneously, directly affecting the degree of springback and the strength of the formed components [3-5]. Hence, there is great interest in analysing the mechanisms and predicting the stress-relaxation ageing (SRA) behaviour in both elastic and plastic strain regimes and at different ageing temperatures. This is a key task to enable accurate simulation and successful optimisation of SRAF processes [6, 7].

In the last few decades, the effects of loading stress on the mechanism and characteristics of SRA or creep-ageing in aluminium alloys have been extensively investigated. Most of the studies focus on the SRA behaviour in the elastic region at a single ageing temperature for SRAF process [8, 9]. It is generally believed that at the ageing temperatures (around $0.5T_m$, where T_m is the absolute melting temperature of the alloys), creep deformation is dominated by dislocation-related mechanisms rather than, for example, grain boundary sliding, the power-law equation has been well developed to analyse the steady-state creep data under SRAF conditions, as [10]:

$$\dot{\varepsilon}_{c\_ss} = A\left(\frac{\sigma}{G}\right)^n \tag{1}$$

where $\dot{\varepsilon}_{c\_ss}$ is the creep strain rate in the steady-state creep stage, A is a temperature dependent parameter, and σ and G are the applied stress and shear modulus respectively. n is the stress exponent, whose value is widely reported to indicate the rate-controlling creep mechanisms [10-12]. By using this creep stress exponent method, the rate-controlling deformation mechanisms in the elastic regime in Al-Zn-Mg alloys at 393 K [13] and Al-Cu-Mg alloys at 438 K [14, 15] have been determined. More recently, attention has been paid to SRA behaviour in the plastic region, during which both initial plastic strains and creep strains are generated, leading to more complicated stress-relaxation behaviour. Recent studies on SRA behaviour in both elastic and plastic regions consider Al-Cu [15], Al-Zn-Mg [16] and Al-Mg-Si [17] alloys.

Results for all these alloys show a much higher level of stress-relaxation when specimens are initially loaded into the plastic region than that into the elastic region. However, when employing the conventional creep exponent method for the stress-relaxation analysis, a negative n value is obtained in the plastic region; this result cannot be explained by current theories. Rong et al. [17] proposed an explanation involving changes in threshold stresses when the material is initially loaded from the elastic region to the plastic region. Yang et al. [15] and Rong et al. [18] further developed models to capture the different stress-relaxation behaviour in the elastic and plastic regions. These results indicated that the conventional creep exponent method was not an adequate description of the different stress-relaxation behaviour and mechanisms in the elastic and the plastic regions.

In addition, the stress-relaxation behaviour and mechanisms demonstrate a strong dependence on temperature, even in the typical ageing temperature range (293 – 573 K) [19-21]. In industrial SRAF of large components, the temperature distribution in the structure during heating and forming may not be uniform. Moreover, some recent studies have proposed non-isothermal SRAF processes to improve the forming efficiency by controlling the heating progress [22, 23]. Some previous studies have qualitatively characterised the effect of ageing temperatures on SRA/creep-ageing behaviour of aluminium alloys [16, 24]. However, quantification of temperature effects and corresponding models are still lacking, limiting the prediction and optimisation of SRAF for advanced aerospace applications under non-isothermal conditions.

Recently, a set of stress-relaxation tests (single and repeated stress-relaxation tests with transient or long-term holding of load) have been developed to determine the governing deformation mechanisms of metals [25-27]. Using these tests, thermally activated deformation-related variables, such as activation volumes and activation energies under certain loading and temperature conditions have been obtained to reveal the detailed thermally activated dislocation mechanisms [28, 29]. In the present paper, the applicability of these tests in analysing and characterising the detailed stress-relaxation behaviour and mechanisms at different temperature and stress levels in both the elastic and the plastic regions is explored. In addition, the quantified deformation-related variables, including activation volumes and energies, could also be utilised to facilitate the modelling of the stress-relaxation behaviour of aluminium alloys and its dependence on stress and temperature.

Hence, in this study, the above-mentioned stress-relaxation test methods and related thermally activated deformation theories are utilised to investigate the long-term SRA behaviour of aluminium alloys for the first time, aiming to provide a new method to characterise the detailed mechanisms and model the SRA behaviour and its dependence on elastic or plastic strain and on temperature. New testing methods have been proposed and applied to characterise the SRA behaviour of an AA7B04 material and obtain deformation-related variables, enabling detailed deformation mechanisms to be determined. Based on the theories developed and the variables obtained in the present work, a new simple constitutive model has been proposed to successfully predict the dependence on temperature and stress of the stress-relaxation behaviour of the alloy, providing a solid tool to support process modelling of industrial forming processes and applications.

2. Theoretical background

The applied shear stress (τ) in a material being plastically deformed, e.g. during stress-relaxation where creep deformation occurs, can be expressed as the sum of two components, an athermal component τ_i and a thermal component τ^* [30, 31]:

$$\tau = \tau_i(\gamma_p) + \tau^*(\dot{\gamma}_p, T), \tag{2}$$

The athermal stress τ_i represents the long-range internal stress in the material that impedes plastic deformation, and is mainly related to the plastic shear strain γ_p. The thermal component τ^* is the effective shear stress leading to plastic deformation, which overcomes the short-range resistance from interactions between dislocations and other dislocations, precipitates and/or solute atoms [14]. τ^*depends on the absolute temperature T and plastic shear strain rate $\dot{\gamma}_p$. For SRA of aluminium alloys at artificial ageing temperatures (around $0.5T_m$) and under intermediate stress levels, dislocations are believed to be the main source of plastic deformation [32]. Hence, the following plastic deformation rate equation can be used [33]:

$$\dot{\gamma}_p = \rho_m b v, \tag{3}$$

where ρ_m is the mobile dislocation density, b is the Burgers vector and v is the average dislocation velocity. An empirical equation describing the power-law dependence of v on the effective shear stress τ^* proposed in [34] is used here, substituting in Eq. (2) to give:

$$v = \alpha(\tau - \tau_i)^m, \tag{4}$$

where α and m are material constants. During SRA, the total strain is held constant, and the stress-relaxation occurs due to that part of the total strain is converted to plastic strain. Hence, the relationship between plastic shear strain rate $\dot{\gamma}_p$ and shear stress-relaxation rate $\dot{\tau}$ can be expressed as:

$$\dot{\gamma}_p = -\frac{\dot{\tau}}{E}, \tag{5}$$

where E is the Young's modulus of the material. By inserting Eqs. (4) and (5) into Eq. (3), one can obtain:

$$-\frac{\dot{\tau}}{E} = \alpha b \rho_m (\tau - \tau_i)^m. \tag{6}$$

The rate equation (Eq. (6)) for the stress-relaxation can be integrated directly with the assumption that τ_i remains constant during a transient stress-relaxation test with a short load holding time, e.g. 10 to 30 s [35]. Thus, the following equation can be obtained by integrating Eq. (6):

$$t = \frac{1}{B(1-m)}\left[\frac{1}{(\tau_0-\tau_i)^{m-1}} - \frac{1}{(\tau-\tau_i)^{m-1}}\right], \tag{7}$$

where t is the stress-relaxation time, τ_0 is the initially applied shear stress and B is a constant. The constants B, m and internal shear stress τ_i can be obtained by fitting Eq. (7) using data from the stress-relaxation curves obtained during transient stress-relaxation tests. It must be noted that m is usually larger than 1 [35]. In addition, with the obtained τ_i values, τ^* can be obtained using Eq. (2).

The physical activation volume V of a material is a property that is widely used to characterise the stress sensitivity of dislocation velocity [31]. For the physical activation volume, repeated stress-relaxation (RSR) tests (Fig. 1) have been invented to characterise the contribution of dislocation velocity on the strain rate [36]. A single stress-relaxation test is followed by a fast reload to the initial stress level, enabling a quasi-elastic condition in the reloading stage, after which, another stress-relaxation stage is performed. As the fast reloading is under quasi-elastic conditions, the dislocation density in the material can reasonably be assumed to be constant. According to the definition of the physical activation ~~energy~~ volume [33],

$$V = kT\frac{\partial \ln(\dot{\gamma}_p)}{\partial \tau} = kT\frac{\ln(\dot{\gamma}_{i2}/\dot{\gamma}_{f1})}{\Delta\tau_1}, \tag{8}$$

in which $\dot{\gamma}_{i2}$ represents the strain rate at the beginning of the second relaxation cycle, $\dot{\gamma}_{f1}$ is the strain rate at the end of the first relaxation cycle and $\Delta\tau_1$ is the total relaxed stress in the first relaxation cycle. As indicated in Fig. 1, the physical activation volume of the materials can be determined with RSR tests. In addition, if each stress-relaxation stage in RSR tests lasts a short time (10 to 30 s), the stress components in Eq. (7) can be obtained from the stress-relaxation curves from RSR tests.

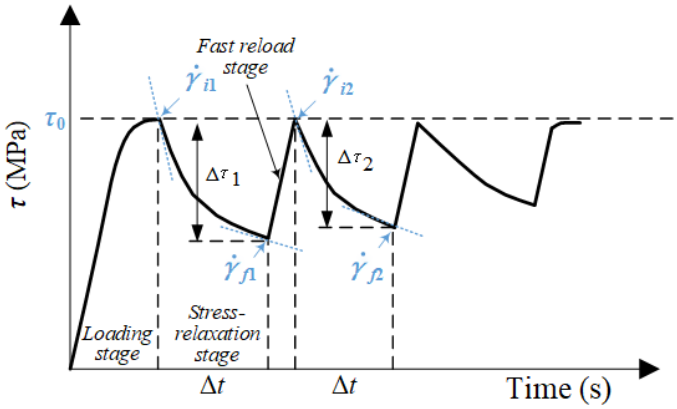

Fig. 1. Schematic showing repeated stress-relaxation (RSR) test procedures.

During stress-relaxation, plastic deformation comes from creep strains (γ_c), and hence $\gamma_p = \gamma_c$. Considering the stress-relaxation curves are obtained under uniaxial tension conditions, the applied shear stress and its components can be converted into normal stresses using the relationship $\tau = \sigma/\sqrt{3}$, $\tau_i = \sigma_i/\sqrt{3}$, $\tau^* = \sigma^*/\sqrt{3}$; and the strain rates are obtained using $\dot{\gamma} = \sqrt{3}\dot{\varepsilon}$ according to the von Mises yield criterion.

Based on the theories summarised above, the athermal (internal stress σ_i) and thermal (effective stress σ^*) normal stress components characterising the creep deformation and the physical activation volume V representing the effect of dislocation velocity can be obtained according to the RSR curves. These data can be used to characterise and analyse the deformation behaviour and mechanisms during SRA of materials [29].

The creep strain rate ($\dot{\varepsilon}_c$) of aluminium alloys can be modelled using the following equation [14]:

$$\dot{\varepsilon}_c = \dot{\varepsilon}_0 \sinh(a\sigma) \exp\left(-\frac{Q_a}{RT}\right) \quad (9)$$

where $\dot{\varepsilon}_0$ is a pre-exponential factor, which can be treated as a material constant. The $\sinh(a\sigma)$ part mainly represents creep strains generated by overcoming the long-range resistance. The other part $\exp(-Q_a/RT)$ represents the thermally activated effect of overcoming the short-

range resistance. R is the universal gas constant and Q_a is the apparent activation energy of the materials, which is strongly affected by the temperature and stress conditions and can be calculated from:

$$Q_a = (\Delta G_0 - V\sigma^*) \quad (10)$$

where ΔG_0 is the Gibbs free energy of activation needed to overcome the short-range resistance at 0 K. Considering that the V and σ^* values can be calculated by fitting the equations introduced before (Eqs. (2), (7) and (8)) to the results of RSR tests, Eqs. (9) and (10) then can be solved for the prediction of creep deformation of a material as a function of stress and temperature conditions. The next section introduces the experiments performed to obtain the values of V, σ^* and Q_a at different temperatures, stress levels and SRA time conditions. Based on these results, a model for the accurate prediction of the stress- and temperature-dependence of SRA behaviour in aluminium alloys is developed and validated.

3. Experiments

3.1 Materials

The heat-treatable 7000 series aluminium alloy AA7B04 (Al-5.97Zn-2.84Mg, wt%), a candidate material to be used for the structural panels in aircraft, was used in this study. The as-received material had undergone solution heat treatment (743 K, 1 h), water quenching, pre-stretch (2%) and artificial ageing (388 K, 8 h), which is named as AA7B04-P in the following sections. The test specimens were machined with the long axis parallel to the rolling direction of the material.

3.2 Mechanical testing programme

Uniaxial tensile tests with a quasi-static loading condition (strain rate of 5 x 10^{-4} /s) were carried out first for the as-received materials at different temperatures (293, 388, 413 and 438 K) to acquire the basic mechanical properties of AA7B04-P; these tests are denoted Group 1 in Table 1.

A set of RSR tests at different stress (or strain) levels and temperatures was designed for the as-received material, in order to determine the stress-relaxation related variables introduced in Section 2 (σ_i, σ_e and V) for analysis and modelling of the stress-relaxation deformation mechanisms. The testing procedures are shown in Fig. 2(a); RSR tests are started when a pre-designated initial stress (or strain) level σ_0 (or ε_0) is attained during tensile loading with a quasi-static condition (strain rate of 5 x 10^{-4} /s). The RSR tests consist of three stress-relaxation

and reloading cycles, with each single stress-relaxation stage lasting 30 s. In each of these cycles, fast reloading is performed after each stress-relaxation stage, with a strain rate of about 5 x 10^{-2} /s to ensure a quasi-elastic reloading state. Three temperatures (388, 413 and 438 K) were used for testing; these cover the main temperatures used for the industrial forming processes. The RSR tests were performed with various pre-designated initial stress (or strain) levels in both elastic and plastic regions (σ_{0i} (or ε_{0i}), (i = 1, 2, …, n) shown in Fig. 2 below). In order to distinguish between elastic and plastic loading conditions in this study, conditions are specified in terms of stress values when loading remains in the elastic region and in terms of strain values when loading is in the plastic region in the following sections. The detailed testing conditions are listed in Table 1, categorised as Group 2, in which $\sigma_{0.01\%}$ and $\varepsilon_{0.2\%}$ represent the 0.01% offset yield strength and 0.2% offset strain respectively.

In addition, in order to investigate the evolution of the stress-relaxation related variables in AA7B04-P during SRA, another set of tests was designed, in which RSR tests were performed on the samples that had been subjected to SRA (SRAed) for different length of time. The detailed test procedures are illustrated in Fig. 2(b). A temperature of 438 K and two initial stress (or strain) levels σ_a (or ε_a), i.e. 200 MPa (elastic region) and 2% (plastic region), were selected for this set of tests. The time of SRA tests (t_1) includes 0.5 min, 10 min, 30 min, 2 h and 4 h. Details of both the SRA tests and the subsequent RSR tests are given in Table 1 as Group 3. Moreover, stress-free ageing (SFA) tests on the as-received AA7B04-P at 438 K and for different time (0.5 min, 2 and 4 h) were performed for comparison, listed as test Group 4 in Table 1. High-temperature tensile tests were carried out directly after SRA or SFA tests without cooling, so as to determine the evolution of high-temperature yield strength of the materials during SRA.

All the tests were performed on an Instron 5584 machine equipped with a furnace. The temperature variations for all tests were controlled within ± 3 K, while the strain of the samples during tests was recorded and controlled by an extensometer (Instron dynamic extensometer 2602-601).

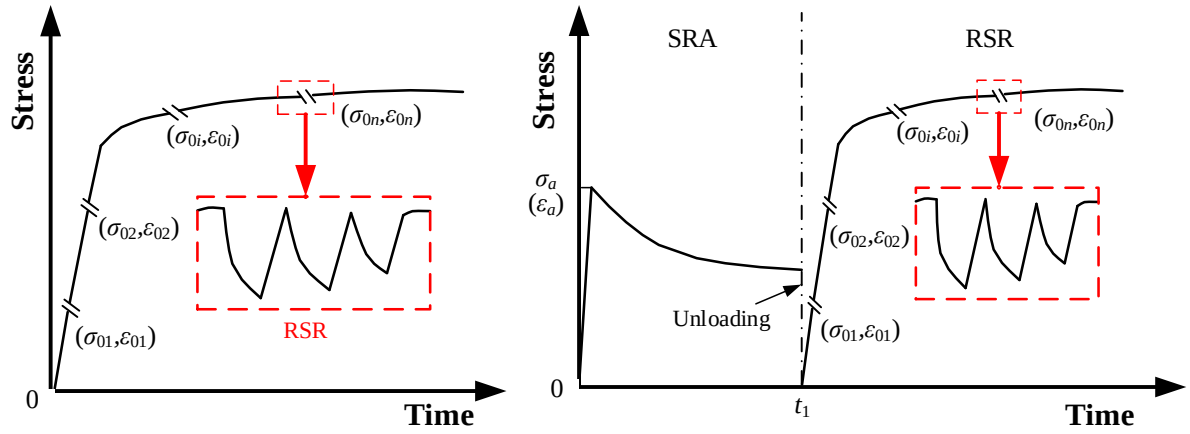

(a) (b)

Fig. 2. Schematic of the mechanical testing procedures. (a) Interrupted tensile tests with repeated stress-relaxation (RSR) and (b) stress-relaxation ageing (SRA) + RSR.

Table 1. Experimental design for the tensile tests, repeated stress-relaxation (RSR) and stress-relaxation ageing (SRA) with subsequent RSR tests.

Procedures	Step1: SRA tests		Step 2: RSR tests	
Variables	ε_a (or σ_a)	Time (t_1)	Temperature	RSR stress (σ_0) or strain values (ε_0)
Group 1	-	-	293, 388, 413, 438 K	- (tensile tests)
Group 2	-	-	388, 413, 438 K	Elastic: 200 MPa, 300 MPa, $\sigma_{0.01\%}$ Plastic: $\varepsilon_{0.2\%}$ ($\sigma_{0.2\%}$), 2%, 4%, 6%
Group 3	200 MPa, 2%	0.5, 10, 30 min, 2, 4 h	438 K	Elastic: 200 MPa, 300 MPa, $\sigma_{0.01\%}$ Plastic: $\varepsilon_{0.2\%}$ ($\sigma_{0.2\%}$), 2%, 4%, 6%
Group 4	-	0.5 min, 2, 4 h	438 K	- (stress free ageing tests)

3.3 Microstructural observations

A JSF-7900F scanning electron microscope (SEM), was used to examine the grain size distributions before and after SRA. SEM samples were cut from the specimens along the loading direction, mechanically ground, and electropolished in a mixture of 10% perchloric acid and 90% methanol at 263 K and 20V. The grain size of the samples was determined using the material image processing and automatic reconstruction (MIPAR) software according to ASTM E112 with the same magnification taken from five randomly selected areas on each sample.

Transmission electron microscopy (TEM) using an FEI Tecnai G2 F20 scanning transmission electron microscope was employed for detailed microstructural examinations in selected specimens after SRA. These included the as-received material and the specimens that had been stress-relaxation aged for 2 and 4 h at 438 K with initial strain values of 0 and 2%. The samples were prepared by cutting to 3 mm diameter discs, mechanically thinning down to 100 μm, and then twin-jet electropolishing with a 20% perchloric acid alcohol solution in methanol maintained at 293 K and 20 V. An FEI Tecnai G2 F20 scanning transmission electron microscope was used for microstructural examination. The dimension of precipitates was quantified by analysing the TEM images of the samples, 4 TEM images from different locations were used for the analysis of each sample.

4. Experimental results and discussion

4.1 Basic mechanical properties

Table 2 presents the basic mechanical properties of the as-received AA7B04-P material at different temperatures, i.e. the Young's modulus (E), 0.2% offset yield strength and corresponding strain ($\sigma_{0.2\%}$, $\varepsilon_{0.2\%}$) and the uniform elongation at which the ultimate tensile strength occurs. In addition, as reported by Lyu et al. [16], the conventional $\sigma_{0.2\%}$ offset yield strength is not the best choice to distinguish between elastic and plastic stress-relaxation behaviour in this alloy. Hence, the recommended 0.01% offset yield strength and corresponding strain ($\sigma_{0.01\%}$, $\varepsilon_{0.01\%}$) are also given in Table 2 and will be used in the following sections to divide the elastic and plastic regions for the stress-relaxation behaviour analysis in this study. As shown in Table 2, the yield strength, Young's modulus and uniform elongation decrease with increasing temperature.

Table 2. Main mechanical properties of the as-received AA7B04-P material at different temperatures.

Temperature	$\sigma_{0.01\%}, \varepsilon_{0.01\%}$	$\sigma_{0.2\%}, \varepsilon_{0.2\%}$	Uniform elongation (%)	Young's modulus (E)
293 K	443 MPa, 0.61 %	512 MPa, 0.94 %	13.9	72.5 GPa
388 K	390 MPa, 0.58 %	461 MPa, 0.94 %	7.7	67.8 GPa
413 K	367 MPa, 0.56 %	429 MPa, 0.90 %	6.3	66.0 GPa
438 K	325 MPa, 0.53 %	387 MPa, 0.81 %	3.7	62.5 GPa

The evolution of the yield strength during SRA tests (from 0.5 min to 4 h in Groups 3 and 4 in Table 1) at 438 K is presented in Fig. 3. With no applied stress, the yield strength of the material increases slightly with increasing ageing time. When the material is initially loaded to give a strain of ε_a = 2%, the yield strength shows an initial increase in the first 10 minutes, and then decreases with increasing SRA time, indicating over-ageing behaviour. The decrease of yield strength during SRA is due to the accelerated precipitation effect which will be shown in the next subsection.

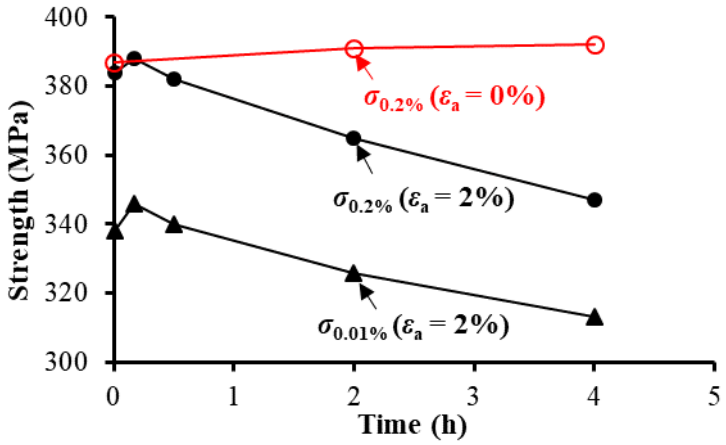

Fig. 3. Evolution of 0.2% proof stress ($\sigma_{0.2\%}$) and 0.01% proof stress ($\sigma_{0.01\%}$) with SRA time at 438 K under initial strain (ε_a) of 0 and 2%.

4.2 Microstructural results

Figs. 4(a) and (b) show representative SEM images of the as-received samples and those subjected to SRA. Elongated grains with an equivalent diameter of 80.1 ± 25.1 μm were observed in the as-received material, whereas after SRA with ε_a = 2 % at 438 K for 4 h, similar grain structures remained with an equivalent diameter of 70.3 ± 17.7 μm. The results show little change in grain size and morphology as a result of SRA, supporting the hypothesis stated in Section 2 that grain-related deformation mechanisms (e.g. grain boundary sliding) have a negligible contribution to deformation behaviour at the ageing temperatures investigated in this study. Fig. 4 (c) to (e) show TEM bright-field (BF) images along the $[110]_{Al}$ zone axis and selected area diffraction (SAD) patterns for the as-received, SFAed and SRAed samples. GP zones and η' and η precipitates are easily observed according to their distinctive morphologies and sizes [37]. Homogenously distributed small precipitates, including GP zones and η', are observed in the as-received material. After 4 h SFA at 438 K, the predominant precipitates in the material are η' and η, the latter is generally larger [37]. For the SRAed specimen under ε_a = 2% at the same temperature and time conditions, much larger rod-shaped η precipitates can

be observed. The average precipitate sizes in the specimens after SFA and SRA are plotted in Fig. 4(f), increasing continuously with ageing time in both cases, while a much higher increasing rate is observed in the SRAed samples. These results show that the external stress (or strain) applied in SRA significantly accelerates precipitation process, leading to coarser precipitates. This is consistent with the results reported by Zhu et al. [38]. The much coarser precipitates in SRAed specimens of AA7B04-P then leads to more significant over-ageing behaviour, giving a decreasing yield strength, observed in Fig. 3.

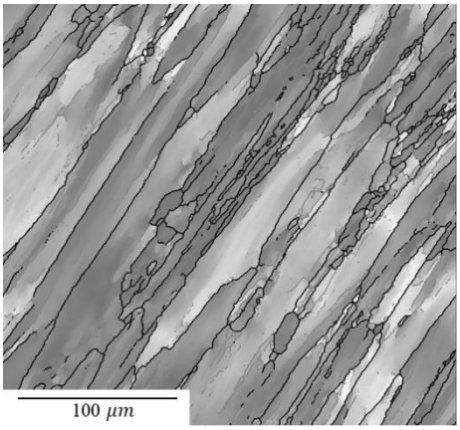

(a)

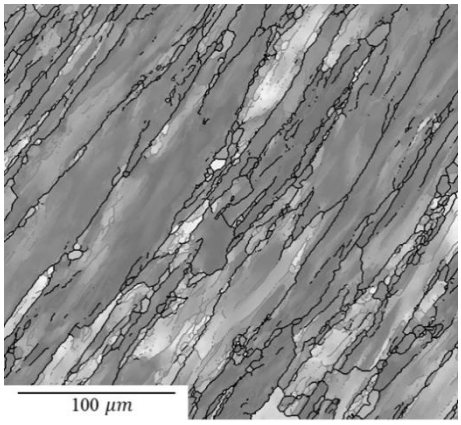

(b)

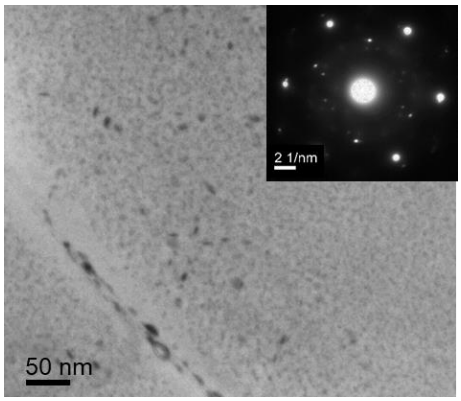

(c)

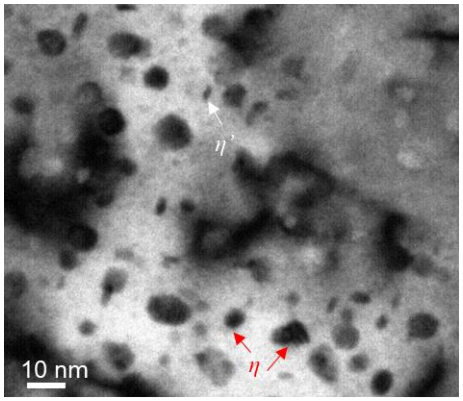

(d)

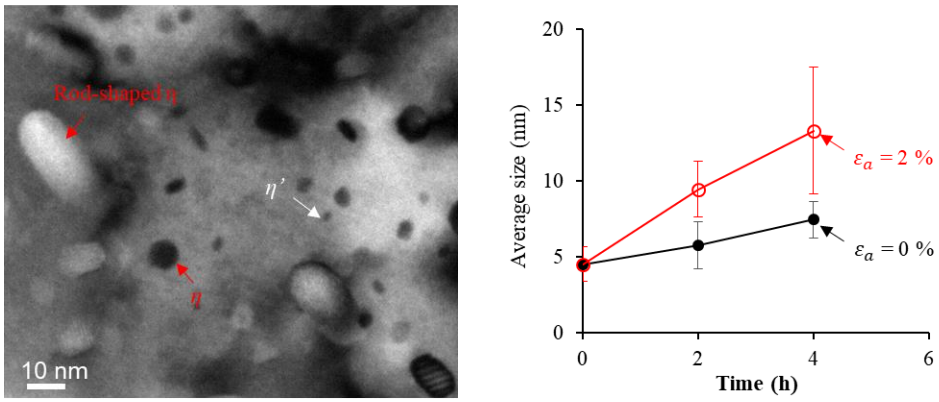

(e) (f)

Fig. 4. Microstructure and precipitate size evolution of AA7B04-P. SEM images showing grains in (a) as-received and (b) 438 K / 4 h SRAed (ε_a = 2 %); TEM BF images and SAD pattern along the $[110]_{Al}$ zone axis showing the distribution of precipitates in (c) the as-received, (d) 438 K / 4 h SFAed (ε_a = 0 %) and (e) 438 K /4 h SRAed (ε_a = 2 %); (f) evolution of average precipitate sizes with ageing time.

4.3 Repeated stress-relaxation behaviour

Fig. 5 shows the three-stage RSR test results of AA7B04-P at 438 K under different stress (or strain) levels (values of $\sigma_{0.01\%}$ and $\varepsilon_{0.2\%}$ are listed in Table 2). A normalised relaxed stress, defined as $\Delta\sigma/\sigma_0$, where $\Delta\sigma = (\sigma_0 - \sigma)$ is the relaxed stress at a transient state, is used to denote the stress-relaxation percentage. Overall, a larger stress-relaxation percentage is observed with increasing initial stress (or strain). In the elastic region, the effect of the initial stress on the normalised relaxed stress is small, with 1.39% of the stress relaxed after 30 s with an initial stress of 200 MPa, compared with 1.73% for an initial stress of $\sigma_{0.01\%}$ (325 MPa). In the plastic region, the initial stress effect on the normalised relaxed stress becomes more significant: 4.2% of stress is relaxed with an initial strain of $\varepsilon_{0.2\%}$, increasing to 8.0% with an initial strain of 6%.

In the three-stage RSR period at 438 K, the relaxed stress percentage decreases with increasing number of cycles except in the case of the initial strains of 2 and 6%. This could be due to the accumulated dislocations in the material from creep deformation in the previous stress-relaxation cycles; these would increase the stress needed for further deformation and lead to the lower degrees of stress-relaxation. When the initial strain is 2%, the relaxed stress percentage remains almost the same. However, when the initial strain is 6%, the relaxed stress

percentage increases with increasing cycle number, as shown in Fig. 5(b). As the uniform elongation of the material at 438 K is 3.7% (Table 2), necking has already occurred at such a high initial strain level of 6%. The necking-related defects in the material could contribute to the increase of relaxed stress percentages with increasing relaxation cycles.

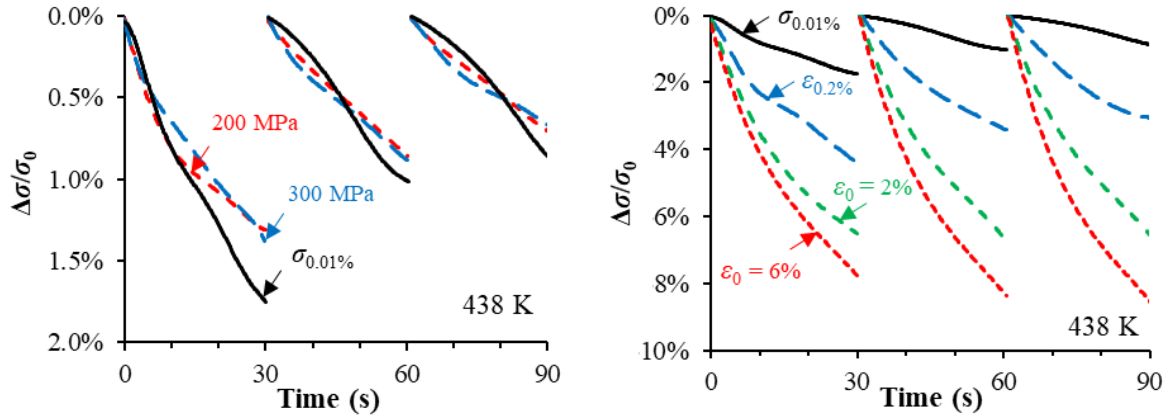

(a) (b)

Fig. 5. Normalised RSR behaviour of AA7B04-P under indicated initial stress (or strain) levels at 438 K: (a) in the elastic region ($\leq \sigma_{0.01\%}$) and (b) in the plastic region.

The normalised RSR curves for selected initial stress and strain levels and different temperatures are compared in Fig. 6. Under all initial stress and strain conditions, a higher temperature leads to a larger relaxed stress percentage. No abnormal increase in relaxed stress percentage with increasing number of relaxation cycles is observed at 388 and 413 K for up to 6% strain at both temperatures, the uniform elongation values are larger than 6%, as given in Table 2, indicating that hardening resulting from dislocation accumulation is still the dominant mechanism during initial loading.

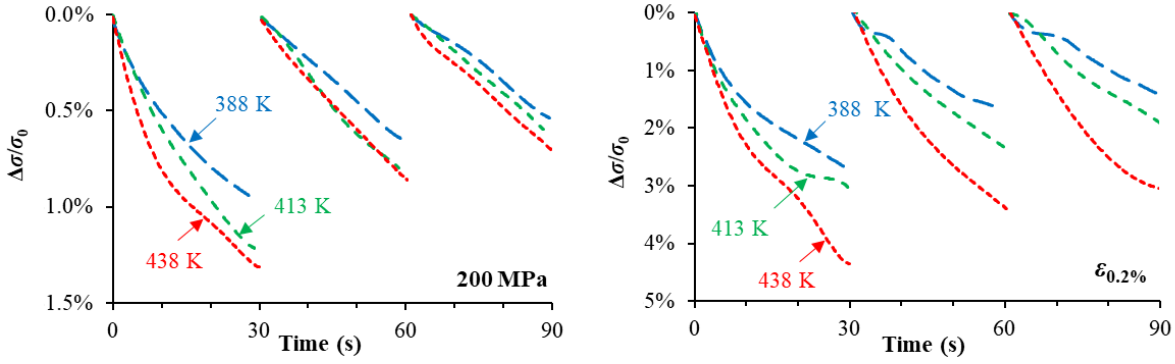

(a) (b)

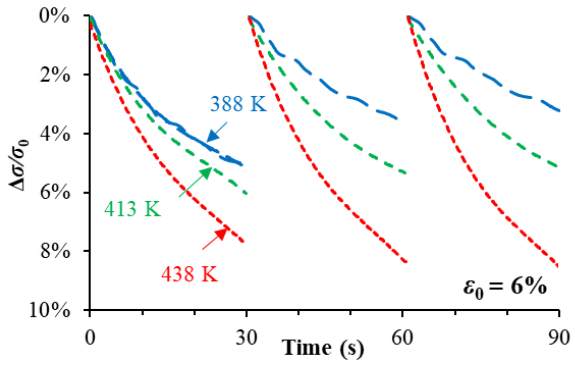

(c)

Fig. 6. Normalised RSR behaviour of AA7B04-P at indicated temperatures under initial stress (strain) of (a) σ_0 = 200 MPa (elastic region), (b) $\varepsilon_0 = \varepsilon_{0.2\%}$ and (c) ε_0 = 6%.

The normalised first-cycle stress-relaxation behaviour of AA7B04-P SRAed under ε_a = 2% for various time is compared in Fig. 7. When the material is loaded with an initial stress of σ_0 = 200 MPa (elastic region) in the RSR tests, the stress-relaxation behaviour appears almost independent of SRA time, as shown in Fig. 7(a). With an initial strain of ε_0 = 2% (plastic region), a slight effect can be recognised with the ageing time, namely that the relaxed stress percentage during RSR decreases slightly after 10 minutes SRA, and then increases with increasing SRA time. This is similar to the trend observed in the yield strength curve in Fig. 3. These results thus indicate that in the elastic region, the SRA time in the range studied has almost no effect on the normalised relaxed stress level, while in the plastic region, a small effect can be observed, which could be related to the yield strength evolutions of the material during SRA.

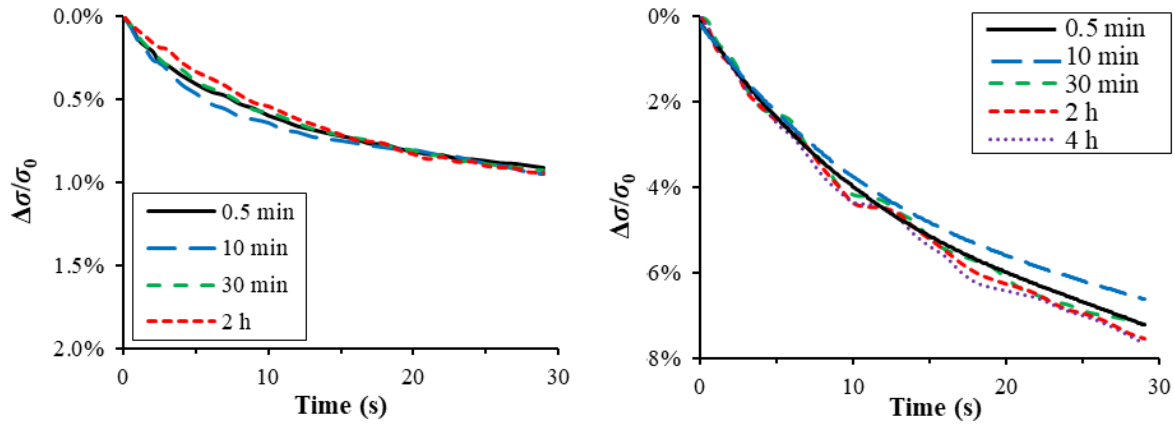

(a) (b)

Fig. 7. Normalised first-cycle stress-relaxation behaviour of SRAed AA7B04-P (ε_a = 2%) after indicated time at 438 K: (a) σ_0 = 200 MPa (elastic region) and (b) ε_0 = 2% (plastic region).

5. Discussion on variables related to stress-relaxation

Using the RSR curves presented in the above sections, key variables related to the stress-relaxation, i.e. the effective stress (σ_e) and physical activation volumes (V), can be calculated by fitting the data to the corresponding equations in Section 2. The results of this fitting are presented and discussed in the following sections.

5.1 Effective stresses

Fig. 8(a) shows the variations of the calculated effective stress (σ_e) of AA7B04-P with normalised initial applied strain ratio which is defined as the ratio of the initial strain (ε_0) to the critical strain at the 0.01% offset condition ($\varepsilon_{0.01\%}$) of the material. Using this definition of initial strain ratio, elastic and plastic regions can be uniformly divided by an initial strain ratio of 1, independently of the temperature effects on $\varepsilon_{0.01\%}$ values shown in Table 2. It can be observed from Fig. 8 that higher effective stresses exist with a larger initial strain ratio and at a higher temperature. As introduced in Section 2, the effective stress is the stress component associated with the thermally activated plastic deformation and is directly related to the creep strains generated during SRA. Hence, increasing σ_e values shown in Fig. 8(a) are the origin of the higher stress-relaxation levels observed for larger applied initial strains in Section. 4.3.

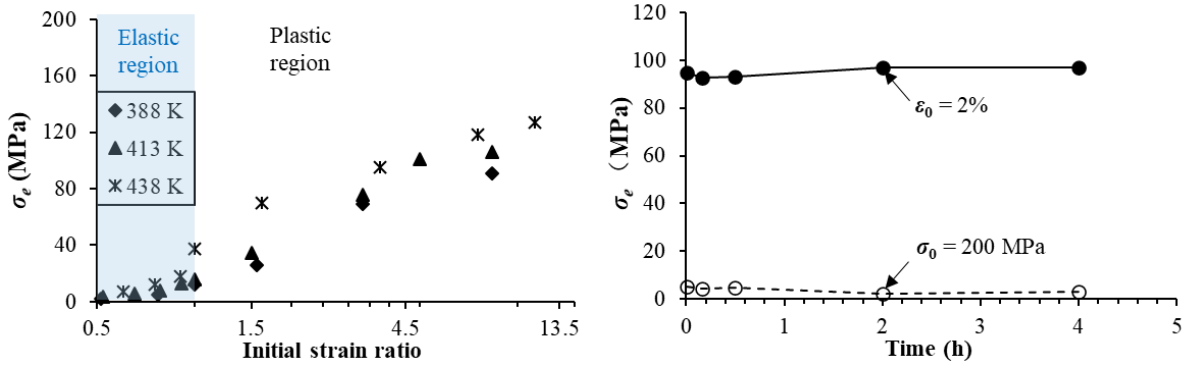

(a) (b)

Fig. 8. Variations of effective stress of (a) AA7B04-P with different initial strain ratios at indicated temperatures and (b) SRAed AA7B04-P (438 K / ε_a = 2%) with time, obtained from RSR tests in the elastic region (σ_0 = 200 MPa) and the plastic region (ε_0 = 2%).

The evolution of the effective stress component of AA7B04-P with SRA time under 438 K / ε_a = 2% are plotted in Fig. 8(b). These results were obtained from RSR tests under initial loads of σ_0 = 200 MPa (elastic) and ε_0 = 2% (plastic). The results indicate that when the material is loaded in the elastic region, effective stresses after SRA show no apparent variations for SRA time of up to 4 h. This corresponds well with the stress-relaxation behaviour observed in these

specimens in Fig. 7(a). Some variations of effective stress with SRA time can be observed in the SRAed alloy when loaded in the plastic region with ε_0 = 2%; this contributes to the small differences of stress-relaxation behaviour shown in Fig. 7(b).

5.2 Physical activation volume

The physical activation volume (V) of AA7B04-P in its as-received state and after SRA for different times is obtained by fitting Eq. (8) to the RSR curves in Section 4.3. Fig. 9(a) shows the variations of V under different initial strains at the three tested temperatures. V value decreases with increasing strain, with a monotonously decreasing speed, and tends to reach a stable level when the initial strain is high enough (about 0.9% for this alloy) in the plastic region. As stated in Section 2, V represents the effect of mobile dislocation velocity on deformation in the loaded alloys. The decreasing V value indicates that enhanced dislocation velocity could be expected in the alloy loaded at higher strain levels [33], which leads to the more significant stress-relaxation of the alloy observed in Figs. 5 and 6. Fig. 9(b) compares the variations of V with initial strains for the materials SRAed with 438 K / ε_a = 2% for different time. Again, from 0 to 4 h SRA time, no significant change V can be observed. These results indicate that the SRA process for up to 4 h investigated in this study has little effect on the physical activation volume, which mainly depends on the initial stress (or strain).

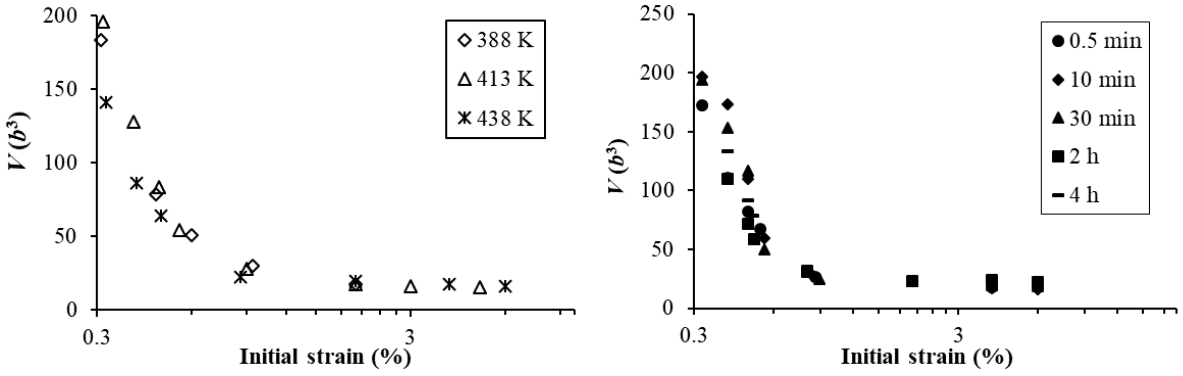

(a) (b)

Fig. 9. Variations of physical activation volume (V) with initial strains for (a) as-received AA7B04-P at indicated temperatures and (b) AA7B04-P SRAed (438 K / ε_a = 2%) with indicated time.

The activation volume has been treated as an effective kinetic signature to indicate the rate-controlling deformation mechanism in thermally activated plastic deformation [31]. For fcc metals with coarse grains, a V value of the order of several hundred b^3 has been reported to indicate a rate-controlling mechanism of forest dislocation interactions during plastic deformation [39]. When the V value is between $1b^3$ and $100b^3$, it is the cross-slip that controls

the deformation [29]. The V values obtained for AA7B04-P in Fig. 9 evolve from more than $200b^3$ at small stress levels in the elastic region to about $10b^3$ at high stress levels in the plastic region, indicating that dislocation interaction is the rate-controlling factor for creep of the alloy at the test temperature range, but the detailed mechanisms may change from forest dislocation interactions at low stresses to cross-slip at high stresses.

An empirical equation proposed in [40, 41] can be adopted to calculate the Gibbs free energy of activation ΔG_0 of the material through the effective stress σ_e and activation volume V, as below:

$$V = \frac{4\Delta G_0}{3\sigma_{e0}}\left[1 - \left(\frac{\sigma_e}{\sigma_{e0}}\right)^{1/2}\right]^{1/2}\left(\frac{\sigma_e}{\sigma_{e0}}\right)^{-1/2} \quad (11)$$

where σ_{e0} is a constant representing the effective stress at 0 K. Fig. 10 shows the relationship between V and σ_e at different strain levels and temperatures for AA7B04-P SRAed for different combinations of temperature and time. A similar trend is observed for all the test conditions, and hence, a value of ΔG_0 = 148 kJ/mol can be obtained for AA7B04-P by fitting the data in Fig. 10 with Eq. (11). This is consistent with previously published values for aluminium alloys, which varies from about 140 to 170 kJ/mol [42, 43].

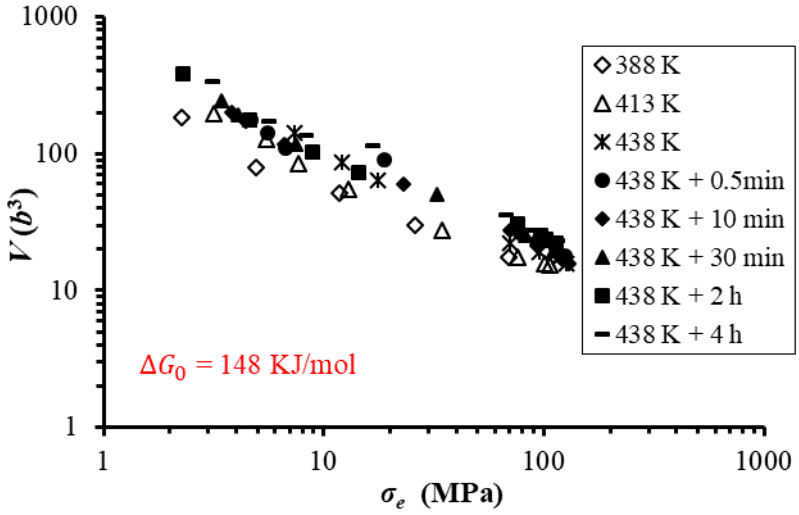

Fig. 10. Physical activation volume (V) vs. effective stress (σ_e) of AA7B04-P SRAed for different combination of temperature and time.

5.3 Activation energy

Using the σ_e, V and ΔG_0 values determined in the previous section, the apparent activation energy values ($Q_a = \Delta G_0 - V\sigma_e$) for AA7B04-P with different stress, temperature and SRA time conditions were calculated and are shown in Figs. 11 and 12. Fig. 11 shows that Q_a

depends strongly on stress and temperature. The variation of Q_a as a function of initial strain shows a similar trend for all three test temperatures. The Q_a value stays at a nearly constant level under different strain levels in the elastic region (Q_{a0}), but starts to decrease quickly with increasing strain levels in the plastic region and tends to reach a stable level when the strain level is high enough. Hence, it can be deduced that the slightly larger stress-relaxation generated with a higher initial stress level in the elastic region in Fig. 5 is mainly due to the external stress, i.e. the $\sinh(a\sigma)$ term in Eq. (9), while the much more significant stress-relaxation behaviour with increasing strain levels in the plastic region is due to the combined effect of increasing applied stress (σ in Eq. (9)) and decreasing apparent activation energy (Q_a in Eq. (9)).

Q_a values also show a temperature dependence in Fig. 11. A higher temperature leads to a smaller Q_{a0}. The relationship between the constant Q_{a0} value in the elastic region and the corresponding temperature is plotted in the insert of Fig. 11, and shows a linear relationship in the range 388 – 438 K. Smaller Q_a values at higher temperatures are the main reason of the higher degree of stress-relaxation at higher temperatures observed in Fig. 6.

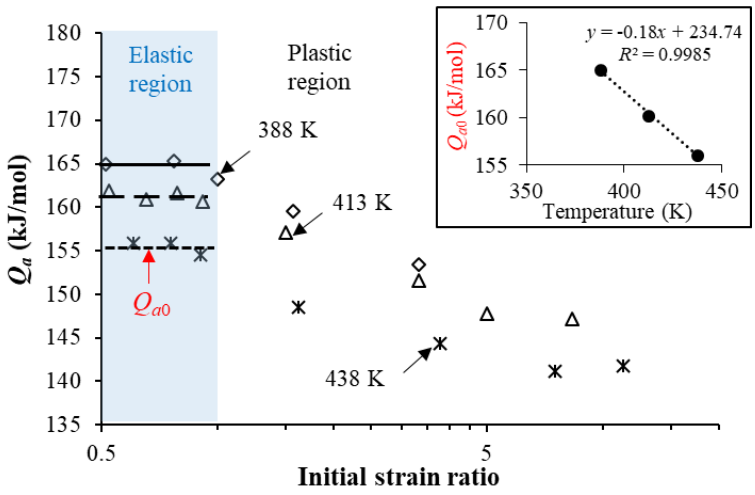

Fig. 11. Evolutions of apparent activation energy (Q_a) of AA7B04-P with initial strain ratios at indicated temperatures (top-right corner insert: average apparent activation energy in the elastic region Q_{a0} vs. temperature).

Fig. 12 shows the variations of Q_a for AA7B04-P with SRA time under 438 K / ε_a = 2%, obtained from RSR tests. Overall, only a slight effect of SRA time on Q_a values is observed. A more pronounce effect can be observed for higher stress levels, with a slight decrease in Q_a value with increasing SRA time. The changing Q_a values should be related to the microstructural evolutions in the alloy during SRA. The additional dislocations introduced by

creep strains in the material during SRA may facilitate further deformation and contribute to a decreasing Q_a values. In addition, the coarser precipitates in the alloy after longer SRA times (from 4.5 nm in the as-received state to the maximum 13.2 nm after 4 h SRA with ε_a = 2% in Fig. 4(f)) could also facilitate dislocation movement and contribute to the decrease in Q_a values with increasing SRA time [44].

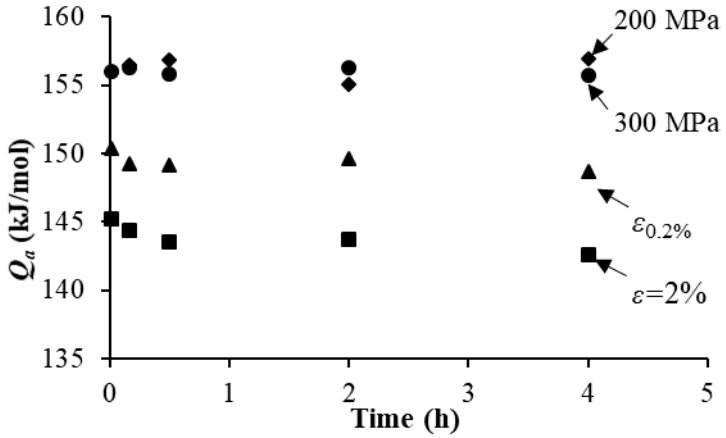

Fig. 12. Evolution of apparent activation energy (Q_a) of AA7B04-P with SRA time under 438 K / ε_a = 2%, obtained from RSR tests under indicated initial stress (strain) levels.

6. Modelling and discussion

The calculated creep-related variables in Section 5 help to elucidate the rate-controlling mechanisms governing deformation of the alloy during SRA and also provide sufficient data for the modelling of the stress-relaxation behaviour of the alloy and its dependence on temperature and stress. The modelling strategy and corresponding results and discussion are introduced in this section.

6.1 Stress and temperature dependent apparent activation energies

According to Eq. (9) in Section 2, the apparent activation energy (Q_a) is the key variable needed for the modelling of creep strain rates during creep or stress-relaxation as a function of temperature. The activation energy Q for dislocation nucleation and propagation in face-centred cubic metals, such as Cu [45], Al and Ni [46] alloys, has been widely investigated previously. The temperature dependence of Q has been experimentally investigated and the following equation has been developed [46]:

$$Q(T) = \left(1 - k_1 \frac{T}{T_m}\right) Q_0 \tag{12}$$

where T_m is the melting temperature of the alloy, k_1 is a material constant and Q_0 is the reference activation energy. The plot of Q_{a0} versus T obtained in this study (Fig. 12), agrees well with the linear relationship between the activation energy Q and the temperature T in Eq. (12) and hence, Eq. (12) is used to model the relationship between Q_{a0} in the elastic region and T as:

$$Q_{a0}(T) = (1 - k_1 T/T_m)Q_0 \tag{13}$$

In the plastic region, the effect of strain (ε_p) on Q_a can be modelled using the equation developed by El et al. [47]:

$$\frac{\dot{Q}_a}{\dot{\varepsilon}_p} = k_2 Q_{a0}(T) - Q_a \tag{14}$$

where k_2 is a material constant.

6.2 Stress-relaxation behaviour under different stresses and temperatures

Using the apparent activation energy, the conventional unified constitutive model proposed for the stress-relaxation behaviour of aluminium alloys in the elastic region at a single temperature [48, 49] is modified to include the effect of temperature and stress in both the elastic and the plastic regions. The new set of constitutive equations is summarised as follows:

$$\begin{cases} \dot{\varepsilon}_c = A_1 \sinh[B_1 \sigma(1-\bar{\rho})] \exp\left(-\frac{Q_a}{RT}\right) \operatorname{sign}(\sigma) \\ \dot{\bar{\rho}} = A_2(1-\bar{\rho})|\dot{\varepsilon}_c| - C_p \bar{\rho}^{m_1} \\ \dot{Q}_a = (k_2 Q_{a0}(T) - Q_a)\dot{\varepsilon}_c \\ \dot{\sigma} = -E\dot{\varepsilon}_c \end{cases} \tag{15}$$

The creep strain rate ($\dot{\varepsilon}_c$) is modelled by the contributions from applied stress (σ), apparent activation energy (Q_a) and normalised dislocation density ($\bar{\rho}$). A_1 and B_1 are material constants. The dislocation density is included in the model in its normalised value ($\bar{\rho}$) in this study, with the same meaning and equation from previous creep-ageing models [48]. A_2 is a constant related to dislocation storage, C_p and m_1 are a constant and an exponent, respectively, related to static recovery. The evolution of the activation energy during stress-relaxation is modelled with the same form as Eq. (14) by considering the dislocation-related creep strains. The stress-relaxation behaviour is then modelled according to the generated creep strains. A_1 and E are temperature-dependent, and can be modelled using the following equations:

$$A_1 = A_{10} \exp\left(\frac{Q_A}{RT}\right) \tag{16}$$

$$E = E_0 \exp\left(\frac{Q_E}{RT}\right) \tag{17}$$

6.3 Model calibration and results

The material constants in the constitutive model developed in Eqs. (12) to (17) are calibrated in this section. The equations developed in this study are mainly based on the basic material equations for creep and stress-relaxation. For the equations with the original form in references, related material constants were directly used. Other material constants in the model were calibrated against corresponding experimental results, including Young's modulus, activation energies and stress-relaxation behaviour obtained in this study. A summary of the proposed model and the calibration procedures used in this study are demonstrated in Fig. 13.

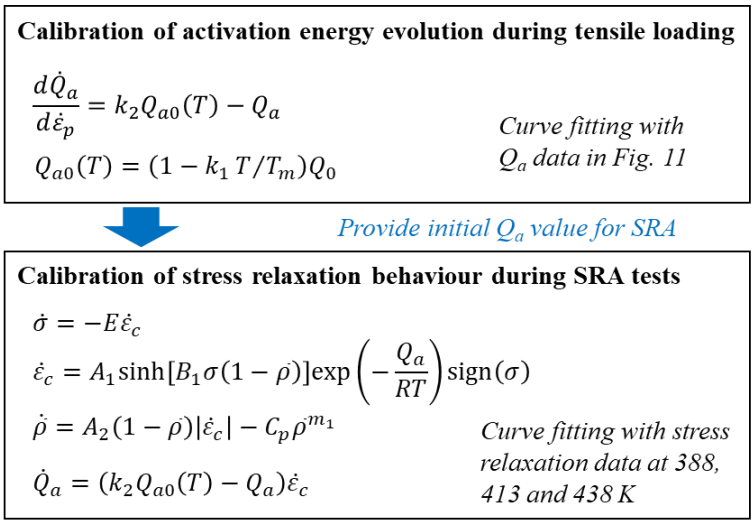

Fig. 13. A summary of the develop model and calibration process for obtaining material constants.

Firstly, the constants in the equations for activation energy (Eqs. (13) and (14)) were calibrated using the data in Fig. 11. Using the calculated activation energy values, the constants in the equations for stress-relaxation behaviour (Eqs. (15) to (17)) were then calibrated. A non-linear least square curve fitting method was employed for the fitting process. The material constants obtained in the two calibration steps are given in Table 3, and the corresponding predicted results are plotted in Figs. 14 and 15.

Table 3. Material constants for the stress-relaxation model of AA7B04-P.

Symbol (unit)	T_m (K)	Q_0 (kJ/mol)	k_1 (-)	k_2 (-)	C_p (s^{-1})	m_1 (-)
Value	930	234.70	0.71	0.91	0.02	1.02
Symbol (unit)	E_0 (GPa)	Q_E (kJ/mol)	A_{10} (s^{-1})	Q_A (kJ/mol)	B_1 (MPa^{-1})	A_2 (s^{-1})
Value	33.8	2.26	0.04	120.70	0.028	220

Fig. 14 compares the model results with corresponding experimental results for Q_a values at different temperatures, initial strain levels and SRA times. In Fig. 14(a), the constant Q_a value in the elastic region and decreasing Q_a with increasing strain in the plastic region are reproduced well by the model, as is the temperature effect. The insignificant effect of SRA time on the variation of Q_a has been modelled by a slight decrease of Q_a along the SRA time in Fig. 14(b). The good agreement between the modelling and experimental results indicate that the model and calibrated material constants show promise for the prediction of apparent activation energies.

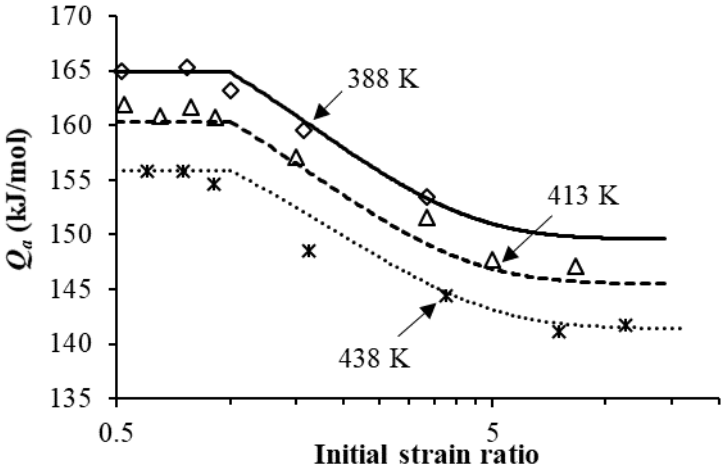

(a)

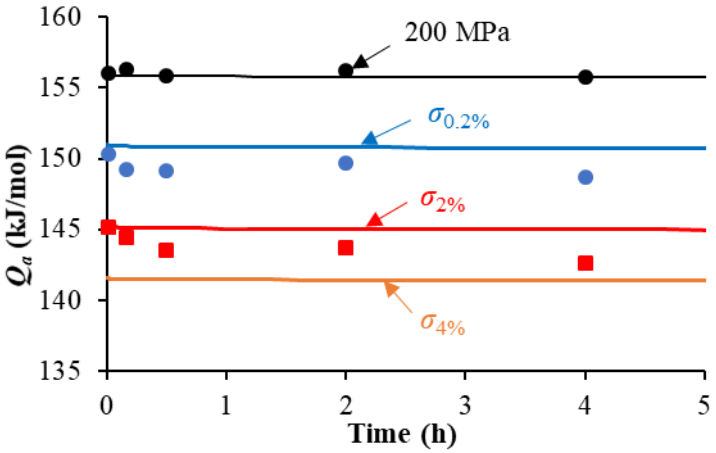

(b)

Fig. 14. Comparison of apparent activation energies (Q_a) from experimental (symbols) and modelling (lines) results of (a) as-received AA7B04-P with different initial strain ratios and temperatures and (b) AA7B04-P SRAed at 438 K / ε_a = 2% for different time, from RSR tests with indicated initial stress levels.

Fig. 15 compares the modelling and experimental results for stress-relaxation at 388, 413 and 438 K for times of up to 5 h, including stresses in the elastic (300 MPa) and the plastic

($\sigma_{2\%}$) regions. The results show that the model reproduced the experimental results accurately for stress-relaxation behaviour under all the test conditions. In addition, the predicted results from the conventional modelling strategy, in which the same stress-relaxation mechanism with a constant Q_a value is used in both the elastic and the plastic regions, are plotted in Fig. 15(b). Comparing the two sets of model results, it can be seen that a significant improvement in prediction accuracy has been achieved using the new model developed in this study. The maximum difference between the modelling and experimental results decreases from over 50% using conventional modelling techniques to only about 6% with the new model, as shown in Fig. 15(b). It can be concluded that the different stress-relaxation mechanisms and corresponding changing Q_a values in the elastic and the plastic regions must be considered to give successful prediction of stress-relaxation behaviour. As it is widely accepted that a higher prediction accuracy for stress-relaxation would lead to a better prediction of springback in formed components after SRAF [1, 50], it is believed that the new model developed in the present work can help to improve the prediction accuracy of springback for SRAF of structural components, especially for stiffened panels preloaded in both the elastic and the plastic regions [2, 16].

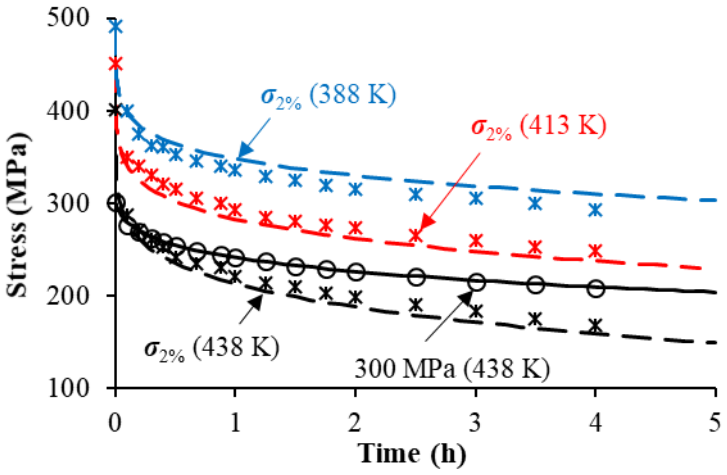

(a)

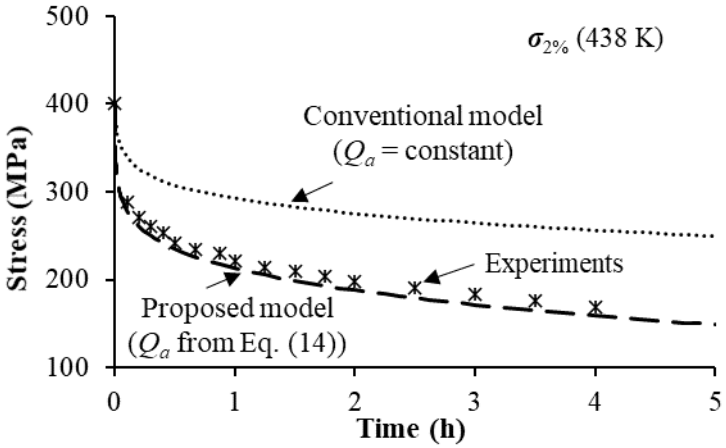

(b)

Fig. 15. Comparison of stress-relaxation curves of AA7B04-P from experimental (symbols) and modelling (lines) results. (a) With selected initial stress and temperature conditions; (b) with conventional and proposed modelling strategies that use the same stress-relaxation mechanism but with a constant or varying Q_a approach for the stress level of $\sigma_{2\%}$ at 438 K.

6.4 Applications for different temperatures and stresses

In order to further validate the capability of the developed model in predicting SRA behaviour of AA7B04-P under different conditions of stress and ageing temperature, the model and corresponding constants in Table 3 have been directly used to predict the stress-relaxation behaviour of the same material at 428, 438 and 448 K under various stress levels in both the elastic and the plastic regions. Experimental data reported in a previous publication [16], none of which was used for calibration of the material constants in the model, was used in this section for comparison and validation.

The detailed stress-relaxation behaviour at 428, 438 and 448 K and under various stress conditions in both the elastic (black symbols and lines) and the plastic (red symbols and lines) regions are compared in Fig. 16. All the modelling results show a very good agreement with corresponding experimental data under all the temperature and initial stress conditions. In addition, it should be mentioned that the stress-relaxation data used for validation is from 18 h SRA tests, which is much longer than the tests carried out in this study (4 h). The model developed using test data from the first 4 h of SRA has successfully predicted the stress-relaxation behaviour in the full 18 h SRA time. It demonstrates the effectiveness of the new model for the accurate prediction of stress-relaxation behaviour of AA7B04-P under different conditions in stress, temperature and SRA time.

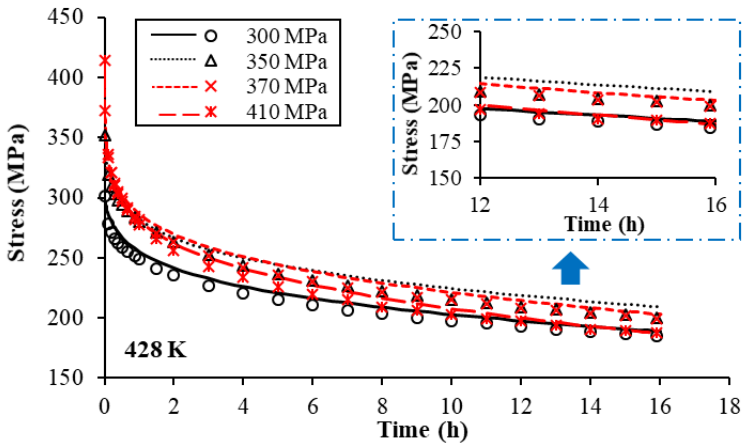

(a)

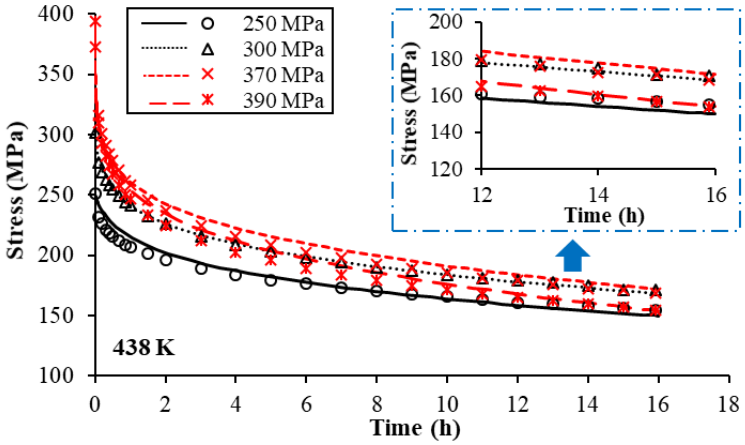

(b)

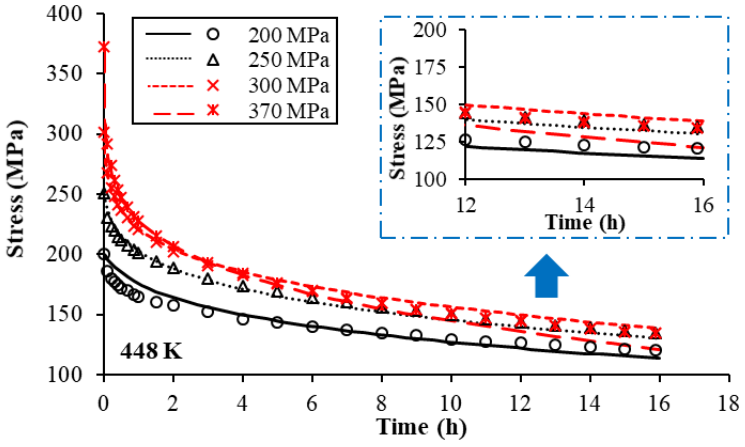

(c)

Fig. 16. Comparison of experimental (symbols, [16]) and modelling (lines) results of stress-relaxation of AA7B04-P under different initial stress levels (elastic: symbols and lines in black; plastic: symbols and lines in red) at (a) 428 K, (b) 438 K and (c) 448 K.

Moreover, in addition to SRA under conventional isothermal conditions, the model developed in the present work enables, for the first time, the prediction of evolutions of stress-

relaxation behaviour in advanced non-isothermal SRA processes. Fig. 17 compares the stress-relaxation results predicted by the developed model for the isothermal (388, 428 and 448 K) SRA processes with an applied stress of 300 MPa with non-isothermal SRA processes with the same applied stress. For the non-isothermal conditions, a linear increase in the temperature from an initial value of 373, 338 or 428 K to a final 448 K during the 16 h SRA process has been assumed for demonstration. When the temperature increases from 428 to 448 K during the 16 h SRA process, a similar trend with decreasing stress-relaxation rate is observed as in the isothermal case, and the relaxation curve is located between the isothermal 428 and 448 K conditions, which is reasonable as the temperature during the non-isothermal SRA is always between 428 to 448 K. When the starting temperature is further decreased, as in the 293 and 338 K conditions shown in Fig. 17, stress-relaxation curves with an increasing rate during SRA are predicted; this behaviour is different from that under isothermal conditions, and is associated with the lower stress-relaxation rate at low temperatures, as illustrated by the stress-relaxation curve at isothermal 338 K in Fig. 17. This predicted behaviour under non-isothermal conditions would definitely affect the final deformation and springback of the components after forming, but could not be predicted by conventional SRA models considering only the isothermal condition.

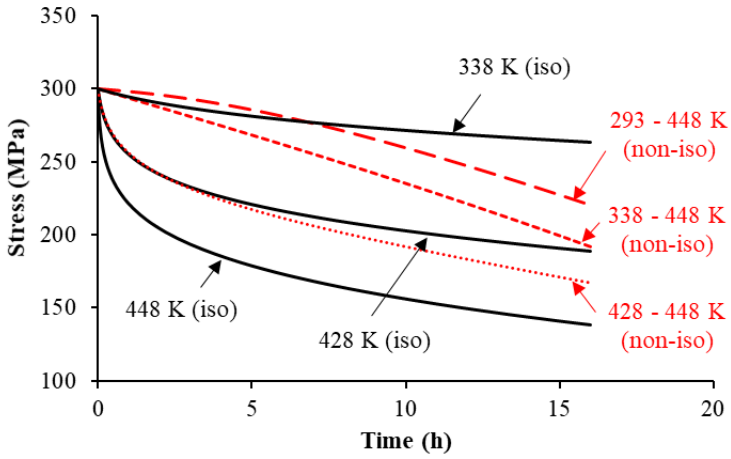

Fig. 17. Comparison of the stress-relaxation behaviour of AA7B04-P under isothermal (iso) and non-isothermal (non-iso) conditions. For non-iso, "xxx – 448 K" represents a linear increase of temperature from xxx K to 448 K during the 16 h SRA.

The model developed in this study considers the dependence of activation energies on stress and temperature, providing a simple and effective way to predict the effects of a wide range of stress, temperature and time conditions on stress-relaxation behaviour of aluminium alloys during SRA. The model has the potential for application to the prediction of creep or stress-

relaxation behaviour at temperatures higher than ageing processes. In addition, by combining the equations for yield strength from the conventional creep-ageing unified constitutive equations [48], this model can be easily extended to concurrently predict shapes (creep/stress-relaxation) and mechanical properties (yield strength) of aluminium alloys for advanced non-isothermal SRAF processes. Moreover, the equations used in this study are mainly based on the basic material equations for creep or stress-relaxation of aluminium alloys, whose applicability in different kinds of heat-treatable aluminium alloys (2xxx, 6xxx and 7xxx) have been illustrated previously [6, 17, 51]. Hence, the model developed in this study could be used for other heat-treatable aluminium alloys with similar stress-relaxation and ageing mechanisms.

7. Conclusions

Based on the theories for thermally activated deformation, a new set of tests combining repeated transient stress-relaxation tests with tensile and long-term stress-relaxation tests have been proposed and performed in this study. The stress components, activation volumes and activation energies of AA7B04 have been quantified for different temperatures, stresses and SRA times, enabling a detailed analysis of deformation mechanisms. Based on the above, a new constitutive model has been developed to effectively predict the stress- and temperature-dependence of SRA behaviour. The following conclusions can be drawn:

1) The more pronounced stress-relaxation behaviour in the plastic loading region than that in the elastic region is caused by the combined effect of higher effective stress and lower apparent activation energy Q_a. The effective stress increases with increasing strain, while Q_a remains constant in the elastic region and decreases with increasing strain in the plastic region. A lower temperature leads to a larger Q_a. In addition, Q_a decreases slightly with increasing time of SRA, especially under higher stresses in the plastic region.
2) The changing physical activation volumes and activation energies indicate a different rate-controlling deformation mechanism of AA7B04-P at low and high stress levels. At low stress levels in the elastic region, a decrease in V from more than $200b^3$ to less than $100b^3$ indicates that forest dislocation interactions play the dominant role in creep deformation and higher temperatures lead to lower V values under the same strain conditions. At high stresses in the plastic region, V values decrease to a few tens of b^3 with more dislocations introduced, indicating that the rate-controlling deformation mechanism turns to cross-slip; the temperature effect on V values then becomes insignificant (between 338 and 438 K investigated in this study).

3) By considering the changing Q_a values under different stress, temperature and time conditions, a novel unified constitutive model has been proposed in this study. Physically-based equations with simple forms have been developed and calibrated, with which the stress level, temperature and time dependent stress-relaxation behaviour of AA7B04-P has been successfully predicted with a high degree of accuracy. The prediction error of stress-relaxation behaviour in the plastic region has been significantly improved from over 50%, using the conventional modelling strategy, to 6% in the present work by considering the different Q_a values in the elastic and the plastic regions.

Data availability

The raw/processed data required to reproduce these findings cannot be shared at this time as the data also forms part of an ongoing study.

Acknowledgements

The research in this paper was funded by the National Natural Science Foundation of China (52005020) and Guangdong Basic and Applied Basic Research Foundation (2019A1515110851). The strong support from the Aviation Industry Corporation of China (AVIC) Manufacturing Technology Institute (MTI) for this research (MESM_P42748) is much appreciated. The authors would like to thank Professor Jianguo Lin and Dr Victoria Yardley from Imperial College London for helpful discussions on this paper

Conflict of interest

On behalf of all authors, the corresponding author states that there is no conflict of interest.

References:

[1] L. Zhan, J. Lin, T.A. Dean, A review of the development of creep age forming: Experimentation, modelling and applications, Int. J. Mach. Tools Manuf. 51(1) (2011) 1-17.

[2] Y. Yang, L. Zhan, R. Shen, J. Liu, X. Li, M. Huang, D. He, Z. Chang, Y. Ma, L. Wan, Investigation on the creep-age forming of an integrally-stiffened AA2219 alloy plate: experiment and modeling, Int. J. Adv. Manuf. Tech. 95(5) (2018) 2015-2025.

[3] G. Henaff, G. Odemer, G. Benoit, E. Koffi, B. Journet, Prediction of creep–fatigue crack growth rates in inert and active environments in an aluminium alloy, Int. J. Fatigue 31(11) (2009) 1943-1951.

[4] L. Kloc, V. Sklenička, P. Dymáček, J. Plešek, New creep constitutive equation for finite element modelling including transient effects, Mech. Mater. 119 (2018) 49-55.

[5] Y. Lin, J.-L. Zhang, G. Liu, Y.-J. Liang, Effects of pre-treatments on aging precipitates and corrosion resistance of a creep-aged Al–Zn–Mg–Cu alloy, Mater. Des. 83 (2015) 866-875.

[6] Y. Li, Z. Shi, J. Lin, Y.-L. Yang, Q. Rong, Extended application of a unified creep-ageing constitutive model to multistep heat treatment of aluminium alloys, Mater. Des. 122 (2017) 422-432.

[7] Y. Lin, G. Liu, M.-S. Chen, J. Li, M. Zhou, H.-M. Zhou, Effects of two-stage creep-aging processing on mechanical properties of an Al–Cu–Mg alloy, Mater. Des. 79 (2015) 127-135.

[8] Y. Li, Z. Shi, J. Lin, Y.L. Yang, B.M. Huang, T.F. Chung, J.R. Yang, Experimental investigation of tension and compression creep-ageing behaviour of AA2050 with different initial tempers, Mater. Sci. Eng. A 657 (2016) 299-308.

[9] Z. Ma, L. Zhan, C. Liu, L. Xu, Y. Xu, P. Ma, J. Li, Stress-level-dependency and bimodal precipitation behaviors during creep ageing of Al-Cu alloy: Experiments and modeling, Int. J. Plast. 110 (2018) 183-201.

[10] M.E. Kassner, Chapter 2 - Five-Power-Law Creep, in: M.E. Kassner (Ed.), Fundamentals of Creep in Metals and Alloys (Third Edition), Butterworth-Heinemann, Boston, 2015, pp. 7-102.

[11] U. Kocks, Laws for work-hardening and low-temperature creep, J. Eng. Mater. Technol. 98(1) (1976) 76-85.

[12] Z. Kowalewski, D. Hayhurst, B. Dyson, Mechanisms-based creep constitutive equations for an aluminium alloy, J. Strain. Anal. Eng. Des. 29(4) (1994) 309-316.

[13] J. Chen, J. Jiang, L. Zhen, W. Shao, Stress relaxation behavior of an Al–Zn–Mg–Cu alloy in simulated age-forming process, J. Mater. Process. Technol. 214(4) (2014) 775-783.

[14] L. Zhan, Z. Ma, J. Zhang, J. Tan, Z. Yang, H. Li, Stress relaxation ageing behaviour and constitutive modelling of a 2219 aluminium alloy under the effect of an electric pulse, J. Alloys Compd. 679 (2016) 316-323.

[15] Y. Yang, L. Zhan, C. Liu, X. Wang, Q. Wang, Z. Tang, G. Li, M. Huang, Z. Hu, Stress-relaxation ageing behavior and microstructural evolution under varying initial stresses in an Al–Cu alloy: Experiments and modeling, Int. J. Plast. (2019) 102646.

[16] F. Lyu, Y. Li, Z. Shi, X. Huang, Y. Zeng, J. Lin, Stress and temperature dependence of stress relaxation ageing behaviour of an Al–Zn–Mg alloy, Mater. Sci. Eng. A 773 (2020) 138859.

[17] Q. Rong, Y. Li, Z. Shi, L. Meng, X. Sun, X. Sun, J. Lin, Experimental investigations of stress-relaxation ageing behaviour of AA6082, Mater. Sci. Eng. A 750 (2019) 108-116.

[18] Q. Rong, Z. Shi, Y. Li, J. Lin, Constitutive modelling and its application to stress-relaxation age forming of AA6082 with elastic and plastic loadings, J. Mater. Process. Technol. 295 (2021) 117168.

[19] F. Nový, M. Janeček, R. Král, Microstructure changes in a 2618 aluminium alloy during ageing and creep, J. Alloys Compd. 487(1) (2009) 146-151.

[20] Z. Li, Z. Li, Z. Tan, D.-B. Xiong, Q. Guo, Stress relaxation and the cellular structure-dependence of plastic deformation in additively manufactured AlSi10Mg alloys, Int. J. Plast. 127 (2020) 102640.

[21] H. Gao, S. Wu, Q. Wu, B. Li, Z. Gao, Y. Zhang, S. Mo, Experimental and simulation investigation on thermal-vibratory stress relief process for 7075 aluminium alloy, Mater. Des. 195 (2020) 108954.

[22] Y. Xu, L. Zhan, M. Huang, R. Shen, Z. Ma, L. Xu, K. Wang, X. Wang, Deformation behavior of Al-Cu-Mg alloy during non-isothermal creep age forming process, J. Mater. Process. Technol. 255 (2018) 26-34.

[23] C. Lei, H. Li, J. Fu, T.J. Bian, G.W. Zheng, Non-isothermal creep aging behaviors of an Al-Zn-Mg-Cu alloy, Mater. Charact. 144 (2018) 431-439.

[24] J. Zhang, Y. Deng, X. Zhang, Constitutive modeling for creep age forming of heat-treatable strengthening aluminum alloys containing plate or rod shaped precipitates, Mater. Sci. Eng. A 563 (2013) 8-15.

[25] M. Hiratani, H.M. Zbib, M.A. Khaleel, Modeling of thermally activated dislocation glide and plastic flow through local obstacles, Int. J. Plast. 19(9) (2003) 1271-1296.

[26] M.S. Mohebbi, A. Akbarzadeh, Y.-O. Yoon, S.-K. Kim, Stress relaxation and flow behavior of ultrafine grained AA 1050, Mech. Mater. 89 (2015) 23-34.

[27] X.-S. Yang, H.-R. Zhai, H.-H. Ruan, S.-Q. Shi, T.-Y. Zhang, Multi-temperature indentation creep tests on nanotwinned copper, International Journal of Plasticity 104 (2018) 68-79.

[28] Z. Trojanová, K. Máthis, P. Lukáč, G. Németh, F. Chmelík, Internal stress and thermally activated dislocation motion in an AZ63 magnesium alloy, Mater. Chem. Phys. 130(3) (2011) 1146-1150.

[29] T. Zhu, J. Li, S. Ogata, S. Yip, Mechanics of ultra-strength materials, MRS Bull. 34(3) (2009) 167-172.

[30] A. Seeger, J. Diehl, S. Mader, H. Rebstock, Work-hardening and work-softening of face-centred cubic metal crystals, Philos. Mag. 2(15) (1957) 323-350.

[31] L. Lu, T. Zhu, Y. Shen, M. Dao, K. Lu, S. Suresh, Stress relaxation and the structure size-dependence of plastic deformation in nanotwinned copper, Acta Mater. 57(17) (2009) 5165-5173.

[32] M.F. Ashby, A first report on deformation-mechanism maps, Acta Metall. 20(7) (1972) 887-897.

[33] J. Martin, T. Kruml, Characterizing thermally activated dislocation mobility, J. Alloys Compd. 378(1-2) (2004) 2-12.

[34] W.G. Johnston, J.J. Gilman, Dislocation velocities, dislocation densities, and plastic flow in lithium fluoride crystals, J. Appl. Phys. 30(2) (1959) 129-144.

[35] T. Kruml, O. Coddet, J. Martin, About the determination of the thermal and athermal stress components from stress-relaxation experiments, Acta Mater. 56(3) (2008) 333-340.

[36] C. Cochrane, T. Skippon, M.R. Daymond, Effect of rate on the deformation properties of metastable β in a high Sn content zirconium alloy, Int. J. Plast. 119 (2019) 102-122.

[37] T.-F. Chung, Y.-L. Yang, B.-M. Huang, Z. Shi, J. Lin, T. Ohmura, J.-R. Yang, Transmission electron microscopy investigation of separated nucleation and in-situ nucleation in AA7050 aluminium alloy, Acta Mater. 149 (2018) 377-387.

[38] A.W. Zhu, J. Chen, E.A. Starke, Precipitation strengthening of stress-aged Al–xCu alloys, Acta Mater. 48(9) (2000) 2239-2246.

[39] S. Mishra, V.K. Beura, A. Singh, M. Yadava, N. Nayan, Effect of Temper Condition on Stress Relaxation Behavior of an Aluminum Copper Lithium Alloy, Metall. Mater. Trans. A 49 (2018) 2631-2643.

[40] R. Kapoor, S.L. Wadekar, J.K. Chakravartty, Deformation in Zr–1Nb–1Sn–0.1Fe using stress relaxation technique, Mater. Sci. Eng. A 328(1) (2002) 324-333.

[41] U. Kocks, A. Argon, M. Ashby, B. Chalmers, J. Christian, T. Massalski, Thermodynamics and Kinetics of Slip, Prog. Mater. Sci. 19 (1975) 1-281.

[42] P. Juijerm, I. Altenberger, Effect of temperature on cyclic deformation behavior and residual stress relaxation of deep rolled under-aged aluminium alloy AA6110, Mater. Sci. Eng. A 452 (2007) 475-482.

[43] A. Deschamps, Y. Brechet, Influence of predeformation and ageing of an Al–Zn–Mg alloy—II. Modeling of precipitation kinetics and yield stress, Acta Mater. 47(1) (1998) 293-305.

[44] A. Takahashi, N.M. Ghoniem, A computational method for dislocation–precipitate interaction, J. Mech. Phys. Solids 56(4) (2008) 1534-1553.

[45] T. Zhu, J. Li, A. Samanta, A. Leach, K. Gall, Temperature and Strain-Rate Dependence of Surface Dislocation Nucleation, Phys. Rev. Lett. 100(2) (2008) 025502.

[46] D.H. Warner, W.A. Curtin, Origins and implications of temperature-dependent activation energy barriers for dislocation nucleation in face-centered cubic metals, Acta Mater. 57(14) (2009) 4267-4277.

[47] M. El Mehtedi, F. Musharavati, S. Spigarelli, Modelling of the flow behaviour of wrought aluminium alloys at elevated temperatures by a new constitutive equation, Mater. Des. 54 (2014) 869-873.

[48] Y. Li, Z. Shi, J. Lin, Y.-L. Yang, Q. Rong, B.-M. Huang, T.-F. Chung, C.-S. Tsao, J.-R. Yang, D.S. Balint, A unified constitutive model for asymmetric tension and compression creep-ageing behaviour of naturally aged Al-Cu-Li alloy, Int. J. Plast. 89 (2017) 130-149.

[49] L. Zhan, J. Lin, T.A. Dean, M. Huang, Experimental studies and constitutive modelling of the hardening of aluminium alloy 7055 under creep age forming conditions, Int. J. Mech. Sci. 53(8) (2011) 595-605.

[50] Y. Li, Z. Shi, Y.-L. Yang, Q. Rong, R. Said, P. Saillard, Effects of asymmetric creep-ageing behaviour on springback of AA2050-T34 after creep age forming, Procedia Eng. 207 (2017) 287-292.

[51] F. Lyu, Y. Li, X. Huang, Z. Shi, Y. Zeng, J. Lin, An investigation of creep age forming of AA7B04 stiffened plates: Experiment and FE modelling, J. Manuf. Process. 37 (2019) 232-241.